Human Molecular Genetics, 2013, Vol. 22, No. 6 **1218–1232**
doi:10.1093/hmg/dds529
Advance Access published on December 20, 2012

Chronic pro-oxidative state and mitochondrial dysfunctions are more pronounced in fibroblasts from Down syndrome foeti with congenital heart defects

Claudia Piccoli[1,†], Antonella Izzo[2,†], Rosella Scrima[1], Ferdinando Bonfiglio[2], Rosanna Manco[2], Rosa Negri[2], Giovanni Quarato[1], Olga Cela[1], Maria Ripoli[1], Marina Prisco[3], Flaviana Gentile[4], Gaetano Calì[4], Paolo Pinton[5], Anna Conti[2], Lucio Nitsch[2,†] and Nazzareno Capitanio[1,*,†]

[1]Department of Clinical and Experimental Medicine, University of Foggia, Foggia 71100, Italy, [2]Department of Cellular and Molecular Biology and Pathology and [3]Department of Biological Sciences, University of Naples Federico II, Naples 80131, Italy, [4]Institute of Experimental Endocrinology and Oncology, National Research Council, Naples 80131, Italy and [5]Department of Experimental and Diagnostic Medicine, University of Ferrara, Ferrara 44100, Italy

Received October 27, 2012; Revised and Accepted December 12, 2012

Trisomy of chromosome 21 is associated to congenital heart defects in ∼50% of affected newborns. Transcriptome analysis of hearts from trisomic human foeti demonstrated that genes involved in mitochondrial function are globally downregulated with respect to controls, suggesting an impairment of mitochondrial function. We investigated here the properties of mitochondria in fibroblasts from trisomic foeti with and without cardiac defects. Together with the upregulation of Hsa21 genes and the downregulation of nuclear encoded mitochondrial genes, an abnormal mitochondrial cristae morphology was observed in trisomic samples. Furthermore, impairment of mitochondrial respiratory activity, specific inhibition of complex I, enhanced reactive oxygen species production and increased levels of intra-mitochondrial calcium were demonstrated. Seemingly, mitochondrial dysfunction was more severe in fibroblasts from cardiopathic trisomic foeti that presented a more pronounced pro-oxidative state. The data suggest that an altered bioenergetic background in trisomy 21 foeti might be among the factors responsible for a more severe phenotype. Since the mitochondrial functional alterations might be rescued following pharmacological treatments, these results are of interest in the light of potential therapeutic interventions.

INTRODUCTION

Down syndrome (DS) is characterized by a complex phenotype in which over 80 features occur with various degrees of expression and frequency (1). DS is a major cause of congenital heart defects (CHD) mainly endocardial cushion defects, the most frequent being atrioventricular canal defects followed by ventricular septal defects and tetralogy of Fallot (2). By comparing the gene expression profiles of 10 human hearts from trisomic foeti to five foetal hearts of non-trisomic controls, we previously demonstrated a global upregulation of chromosome 21 (Hsa21) genes and a dysregulation of ∼400 genes localized on other chromosomes (3). Microarray analysis clearly showed the downregulation of genes encoding all five mitochondrial complex subunits and of genes implicated in mitochondrial biogenesis. This suggested that the corresponding proteins and enzymatic activities might be reduced in DS subjects and that mitochondrial function could be consequently impaired.

*To whom correspondence should be addressed at: Department of Clinical and Experimental Medicine, Via Pinto 1 c/o OO.RR., 71100 Foggia, Italy. Tel: +39 881711148; Fax: +39 881714745; Email: n.cap@unifg.it
†The authors wish it to be known that, in their opinion, the first two authors (C.P., A.I.) should be regarded as joint First Authors and that the last two authors (L.N., N.C.) contributed equally to the work.

Trisomy of chromosome 21 has been associated with mitochondrial dysfunction in cells and tissues from DS subjects (4–6) and in mouse models (7,8). These results led to the hypothesis that mitochondrial dysfunction contributes to the DS phenotype. Protein levels of mitochondrial complexes I, III and V were decreased in cerebellar and brain regions of DS subjects (9). Complex I was also deficient in mouse models of trisomy of chromosome 16. The results were similar to those obtained from models of Parkinson's disease, suggesting that different neurodegenerative diseases may be associated with the same mitochondrial dysfunction (10).

Recently, it has been also reported that the mitochondrial energy production apparatus was less efficient in foetal DS fibroblasts, due to the dysregulation of adenine nucleotide translocator, ATP synthase and adenylate kinase, and a selective deficit of complex I, which contributes to reactive oxygen species (ROS) overproduction in DS mitochondria. These events were attributed to changes in the cAMP/PKA signalling pathway (11,12), which is known to affect the abundance of the transcriptional coactivator *PGC-1α* (peroxisome proliferator-activated receptor gamma coactivator 1-alpha). This protein, that plays a central role in regulating mitochondrial biogenesis and respiratory function through the interaction with transcriptional partners, like *NRF1*, *ERRα*, *PPARs* and *YY1*, is negatively controlled by the co-repressor *RIP140*, a gene mapping to Hsa21 (13).

Even though these results are indicative of widespread mitochondrial dysfunction in DS, molecular studies have not yet been performed to investigate the basis of mitochondrial dysfunction at the transcriptional level. Furthermore, no hypotheses have been formulated about the mechanisms by which trisomy of Hsa21 genes might induce such a dysfunction.

The original contribution of the present study consists of a contemporary analysis of mitochondrial features at the molecular, morphological and functional level in 13 human primary lines of foetal fibroblasts (HFF) derived from Hsa21 trisomic foeti, with or without CHD, and from euploid controls. The mitochondrial defects associated with DS were analysed taking into account the regulation of the Hsa21 and mitochondrial-related genes and the cardiac phenotype, in order to identify pathways involved in mitochondrial function and dysrupted by the Hsa21 trisomy. A striking and more severe ROS- and Ca^{2+}-related mitochondrial dysfunction emerged in cardiopathic-derived Hsa21 trisomic fibroblasts, unveiling a more pronounced pro-oxidative state.

RESULTS

The present study combines the molecular, morphological and functional analyses of mitochondria in 13 human primary cultures of HFF. Five were from euploid foeti (N-HFF, N standing for normal), and eight (DS-HFF) were derived from Hsa21 trisomic foeti [four samples from DS foeti with heart defects, named CDS-HFF (CDS standing for Cardiopathic Down Syndrome), and four samples from DS foeti without heart defects, named NCDS-HFF (NCDS standing for Non Cardiopathic Down Syndrome)].

Gene expression is dysregulated in DS-HFF samples

The analysis of HFF karyotypes demonstrated that all trisomic fibroblasts showed three copies of Hsa21 as the only cytogenetic alteration (data not shown). The expression of some Hsa21 genes was determined by quantitative real-time PCR (qRT-PCR) experiments comparing DS-HFF versus N-HFF. In particular, the Hsa21 genes *BTG3*, *SOD1*, *ITSN1*, *DYRK1A*, *NRF2* and *RIP140* were upregulated in trisomic fibroblasts when compared with controls (Fig. 1A), thus confirming the gene dosage effects that was previously demonstrated in human foetal tissues (3,14). We then focused on genes that mapped to chromosomes different from Hsa21 and were involved in multiple mitochondrial functions, such as the respiratory chain, mitochondrial biogenesis and morphology, and genes involved in related pathways, such as the *Calcineurin/NFAT* (Nuclear factor of activated T-cells) axe. Most of the analysed genes were significantly downregulated in trisomic versus euploid fibroblasts (Fig. 1B), demonstrating that trisomy of chromosome 21 perturbs the expression of genes involved in mitochondrial pathways. Moreover, *NFATc3* and *NFATc4* were significantly downregulated while *DYRK1A* and *RCAN1*, two Hsa21 genes involved in regulating the levels of *NFATc* phosphorylation, were upregulated in trisomic versus euploid fibroblasts (Fig. 1C).

Mitochondria of DS-HFF show morphological abnormalities

Electron microscopy (EM) of trisomic fibroblasts revealed that a significant number of mitochondria had an abnormal morphology, showing an increased size, irregular shape, evident breaks, mainly of inner membranes. In addition, the mitochondria showed alterations in the pattern of cristae where some were broadened and arranged concentrically or oriented parallel to the long axis of the organelle (longitudinal cristae) (Fig. 2A). Broken mitochondria and mitochondria with concentric and longitudinal cristae were significantly more abundant in trisomic samples than in the euploid ones ($P < 0.05$) (Fig. 2B). Stereological analysis demonstrated that the mitochondrial volume density, expressed as a percentage of cellular volume, was similar in euploid and trisomic samples while the cristae volume density, expressed as a percentage of mitochondrial volume, was significantly lower in all DS-HFF samples when compared with N-HFF ($P < 0.05$) (Fig. 2C and D).

The functional mitochondrial phenotype is altered in CDS-HFF

Endogenous oxygen consumption rate in intact HFF

The respiratory activity of N-HFF and DS-HFF samples was compared by high-resolution oxymetry. The oxygen consumption rate (OCR) was assessed in intact cells relying on endogenous respiratory substrates and corrected for the residual KCN-sensitive OCR and, therefore, attributable to mitochondrial respiratory chain-dependent activity. Figure 3A shows the results of a systematic analysis whereby the activity of each cellular sample was measured. Although a relatively large inter-individual variability was observed within each of

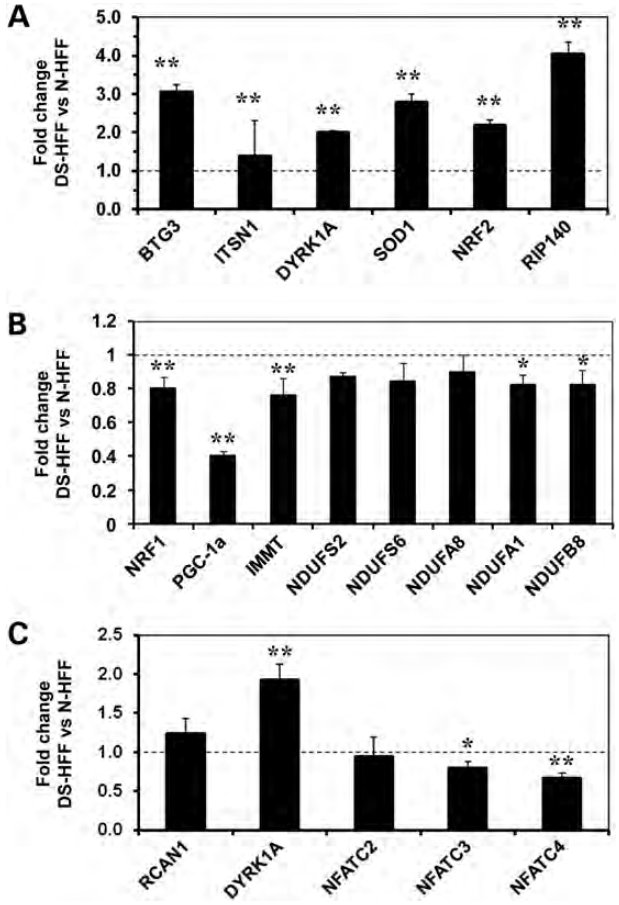

Figure 1. Gene expression is dysregulated in DS fibroblasts. Gene expression fold change in DS-HFF samples versus N-HFF samples for Hsa21 genes (**A**), nuclear-encoded mitochondrial genes (**B**) and calcineurin/NFAT-related genes (**C**) as obtained by qRT-PCR. Values represent the mean of three replicates ± SEM. $^{*}P < 0.05$, $^{**}P < 0.01$, N-HFF, Euploid fibroblasts; DS-HFF, Hsa21 trisomic fibroblasts.

the three groups, on an average basis, the resting respiration of DS-HFF showed a significant decrease that was more evident in CDS-HFF (≈43% inhibition) when compared with N-HFF. Conversely, a slight increase in the OCR in the presence of the FoF1-ATP synthase inhibitor oligomycin was observed in DS-HFF, whereas in the presence of the protonophoric uncoupler FCCP a slight, albeit significant, decrease (≈27% inhibition) in the OCR was observed in CDS-HFF when compared with N-HFF. The respiratory control ratio (RCR), attained by dividing the uncoupled OCR by that in the presence of oligomycin, was as high as 14–16 irrespective of the cell group analysed (Fig. 3B). The ATP-synthase independent OCR (leak) was unchanged between N- and DS-HFF, whereas the oxidative phosphorylation-dependent OCR (OXPHOS) was significantly reduced in DS-HFF, and more specifically in CDS-HFF, by 36% when compared with N-HFF (Fig. 3B). The decrease in OCR_{RR}, observed in DS-HFF, individually correlated to the altered mitochondrial morphology and cristae volume density assessed by EM (Fig. 3C). Next, we measured the mitochondrial membrane potential ($\Delta\Psi_m$) by confocal microscopic imaging using the specific mitotropic probe TMRE. A significant difference was not observed in the TMRE-related fluorescence among N-HFF, NCDS-HFF and CDS-HFF (Fig. 4A), even though a finer analysis of the fluorescent signal revealed a less interdigitated mitochondrial network morphology in DS-HFF (Fig. 4B).

Complex I activity

To assess if the observed respiratory deficit in DS-HFF resulted from a specific defect in one or the other of the respiratory chain complexes, the activity of the protonmotive complexes I, III and IV was measured in cell lysates. The activity of citrate synthase, which is an index of mitochondrial mass, was also measured. Figure 5A shows that the activity of complex I was significantly depressed (by about 50%) in both NCDS-HFF and CDS-HFF when compared with N-HFF. The decreased activity of complex I correlated with the altered mitochondrial cristae morphology. Conversely, significant differences in activities of complexes III and IV were not observed among the three cell groups (Fig. 5B and C). Likewise, the citrate synthase activity was practically unaffected (Fig. 5D); therefore, following normalization to the mitochondrial mass, the selective inhibition of complex I in trisomic cells was confirmed (data not shown). Total protein levels per cell were slightly less in trisomic samples but not to a statistically significance degree compared with N-HFF (Fig. 5E).

Mitochondria-related ROS production

Intracellular ROS level was assessed by confocal microscopy imaging of cells treated with the redox-sensitive fluorescent probe DCF. Every trisomic sample displayed an enhanced ROS production when compared with N-HFF, with a larger redox imbalance in CDS-HFF (Fig. 6A). Enlargement of the confocal images showed a compartmentalized, brighter signal of the DCF-related fluorescence with a very low variability within each group. On an average basis, the ROS-related DCF fluorescence was much larger in CDS-HFF when compared with NCDS-HFF (Fig. 6B). Plotting the DCF fluorescence versus the normalized complex I activity for each individual HFF sample suggested the presence of a threshold value of complex I activity below which extra-ROS production was generated (Fig. 6C). To further ascertain the source of the ROS release in DS-HFF, cells were treated with DPI, which is a pan-inhibitor of flavin-containing oxidases (including complex I). DPI treatment was associated with a marked decrease in the ROS over-production in representative samples of both NCDS- and CDS-HFF, whereas it was ineffective in N-HFF (Fig. 7). Production of ROS by the respiratory chain complex I is fostered by the presence of a $\Delta\Psi_m$ (15). Short-time incubation of cells with the uncoupler FCCP significantly inhibited ROS release both in NCDS- and CDS-HFF with a larger effect in the latter (Fig. 7). It has been recently reported that alteration of PKA-dependent signalling affects functioning of the oxidative phosphorylation (OXPHOS) system (11,16,17). Treatment of cells with the cAMP analogue db-cAMP significantly reduced ROS production in both NCDS- and CDS-HFF although the redox state, especially in CDS-HFF, was not fully renormalized to the level of N-HFF (cf. Fig. 7 with 6B).

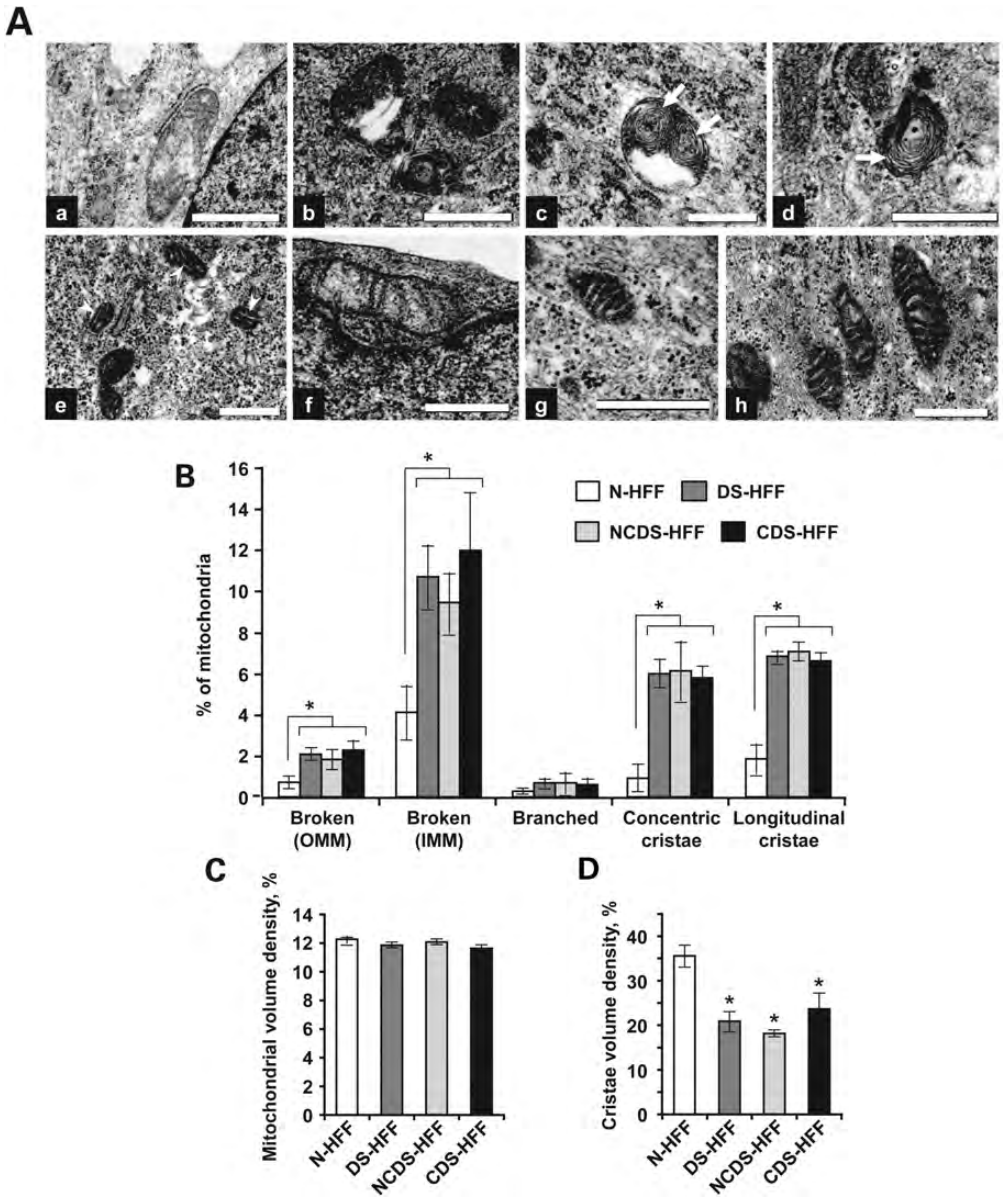

Figure 2. Mitochondria of DS fibroblasts show morphological abnormalities. (**A**) Electron micrographs of morphologically abnormal mitochondria in DS-HFF (a–f) and normal mitochondria in N-HFF (g and h); (a and b) broken mitochondria; (c and d) mitochondria with concentric cristae (arrow); (e) mitochondria with longitudinal cristae (arrow head); (f) mitochondria with significantly reduced cristae; (g and h) mitochondria with unchanged morphology in N-HFF. Scale bars: 500 nm. (**B**) Percentages of mitochondria with abnormal morphology in fibroblasts. (**C**) Mitochondrial volume density relative to cell volume. (**D**) Mitochondrial cristae volume density relative to mitochondrial volume. In (**B**)–(**D**), the mean values ± SEM are shown along with statistical analysis; $^{*}P$ significant cut off < 0.05 Kolmogorov–Smirnov and Kruskall–Wallis tests. N-HFF, euploid fibroblasts; DS-HFF, Hsa21 trisomic fibroblasts; NCDS-HFF, Hsa21 trisomic fibroblasts from DS foeti without heart defects; CDS-HFF, Hsa21 trisomic fibroblasts from DS foeti with heart defects.

Steady-state intra-mitochondrial calcium level

Deregulation of Ca^{2+} homeostasis and Ca^{2+}-mediated signalling has been described in cells derived from trisomic patients or in murine models of DS (18–20). Mitochondria are known to function as a Ca^{2+} buffer by taking up Ca^{2+} mainly via a specific ruthenium red (RR)-inhibitable uniporter (21,22). To verify this point, we evaluated the intramitochondrial level of calcium ($mtCa^{2+}$) using the specific probe Rhod-1. Figure 8A and B shows representative confocal microscopic images of the analysis along with statistical evaluation of the results. It is shown that DS-HFF displayed a statistically significant more intense Rhod-1-related fluorescence signal when compared with N-HFF. However, this was mainly contributed by the CDS-HFF samples. Closer examination of the intracellular fluorescence unveiled a compartmentalization of the brighter signal confirming that it was largely displaying the steady-state $mtCa^{2+}$ level. The enhanced $mtCa^{2+}$ load in DS-HFF correlated positively with the increase in ROS production (Fig. 8C) consistent with the notion that calcium entry in mitochondria induces redox state alterations (23).

To verify the interplay between calcium and ROS, representative trisomic samples were treated with RR and the redox

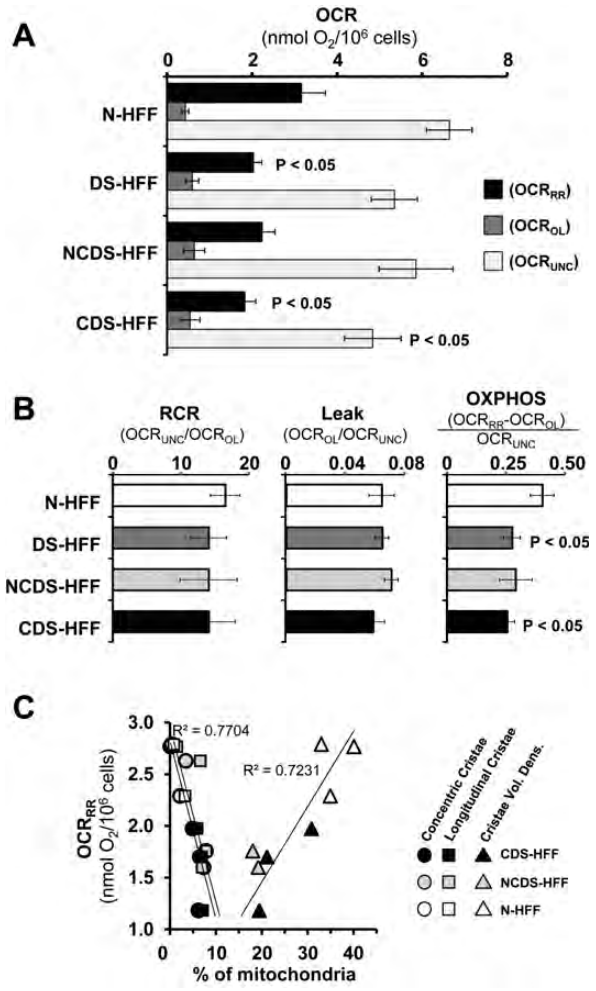

Figure 3. Respirometric analysis in DS fibroblasts. (**A**) OCRs normalized to cell number were assessed by high-resolution oxymetry in intact cells as described in the Materials and Methods. A comparative analysis between five different euploid (N-HFF) and eight different trisomic (DS-HFF) samples is shown; a distinction of the DS-HFF between non-cardiopathic (NCDS-HFF, $n = 4$) and cardiopathic (CDS-HFF, $n = 4$) foetus-derived fibroblasts is also reported. The endogenous OCR were measured under resting conditions (OCR_{RR}), in the presence of oligomycin (OCR_{OL}) and in the uncoupled state in the presence of FCCP (OCR_{UNC}). (**B**) Respiration-linked bioenergetic parameters computed by the OCR measurements shown in (A). RCR, respiratory control ratio; Leak, non-ATP-synthase-controlled respiratory activity; OXPHOS, ATP-synthase-controlled respiratory activity. The bars in (A) and (B) are means ± SEM of the average determinations for each sample carried out at least in triplicate; when statistically significant, the difference when compared with the euploid samples is shown. (**C**) Correlation plots between respiratory activity under resting conditions (OCR_{RR}) and percentage of concentric or longitudinal cristae or of cristae volume density for individual fibroblast samples (see the symbol legend).

state assessed by DCF. As shown in Figure 9A and B, inhibition of the mitochondrial Ca^{2+} porter by RR caused a substantial inhibition of ROS production, suggesting that the entry of Ca^{2+} in the mitochondrial compartment was at least partially responsible for the redox imbalance in trisomic cell samples. Moreover, treatment with RR resulted in enhancement of the respiratory activity in DS-HFF to the level of N-HFF (Fig. 9C). Similar results were obtained evaluating mitochondrial calcium levels by a different method based on a calcium-sensible photoprotein, the aequorin (see Supplementary Material, Text S1 and Fig. S1).

Mitochondrial biogenesis is affected by Hsa21 trisomy

Lastly, to verify if the observed mitochondrial dysfunction was associated to a decreased mitochondrial biogenesis, we quantified the copy number of mitochondrial DNA by absolute qRT-PCR. There was an average value of ∼600 copies per nuclear genome (i.e. per cell) in N-HFF, 500 in NCDS-HFF and 400 in CDS-HFF (Fig. 10A). A statistical significance was attained only for CDS-HFF.

As the mtDNA replication is controlled by *PGC-1α*, which is a master regulator of mitochondrial biogenesis (13), we analysed the correlation between *PGC-1α* expression and the amount of mtDNA. The amount of *PGC-1α* gene transcripts was reduced by ∼40–50% in trisomic samples versus N-HFF (Fig. 10B). Western blotting of *PGC-1α* confirmed at the protein level a significant decrease in NCDS-HFF and an even more marked decrease in CDS-HFF when compared with N-HFF (Fig. 10C). A direct correlation between *PGC-1α* expression and amount of mtDNA was observed in our samples (Fig. 10D).

DISCUSSION

We previously demonstrated that more than 80 genes, encoding mitochondrial enzymes and respiratory chain subunits, are downregulated in foetal trisomic heart tissues (3). Of these genes, 40 % have consensus DNA binding sites for the nuclear respiratory factor *NRF1* in their 5' flanking regions, and 20 % of them show a high affinity for the oestrogen-related receptor *ERRα* (see Supplementary Material, Text S2 and Tables S3 and S4). It has been recently demonstrated that the transcription factors *NRF1* and *ERRα* and their targets are repressed by Hsa21 gene *RIP140* and induced by *PGC-1α* in a dose dependent manner in neonatal rat cardiomyocytes (24). Our results indicate that *NRF1* and *PGC-1α* are significantly downregulated in DS HFF. Western blotting of *PGC-1α* confirmed the downregulation also at the protein level in trisomic fibroblasts. This downregulation correlated well with the downregulation of complex I activity and with the mtDNA copy number decrease (more evidently in CDS-HFF). *PGC-1α* function has been investigated in several specialized cell types and transgenic mouse models, demonstrating its role in the regulation of mitochondrial oxidative metabolism. *PGC-1α* null mice show reduced expression of mitochondrial genes in multiple tissues (25,26). *PGC-1α* controls the expression of nuclear-encoded mitochondrial genes through interactions with its transcriptional partners *NRF1* and *ERRα*, which are also downregulated in DS samples.

Morphological analysis of mitochondria in trisomic versus euploid samples demonstrated ultrastructural changes in DS-HFF mitochondria. These results provide additional evidence of altered mitochondrial morphology observed in DS brain tissues and mouse models (8,27). Silencing experiments demonstrated that the downregulation of *IMMT* causes a drastic change in the organization of the inner membrane

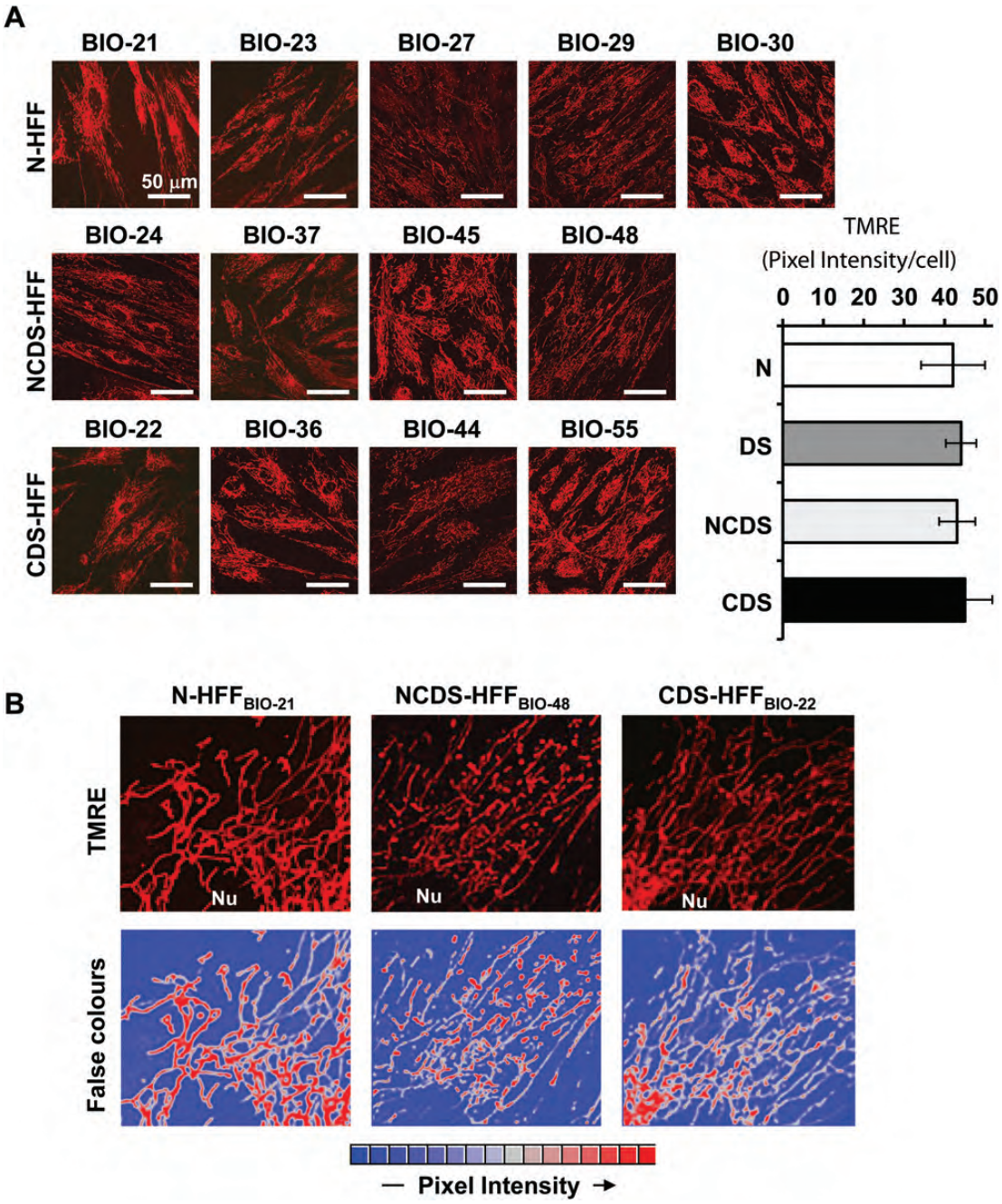

Figure 4. Confocal microscopy analysis of mtΔΨ in DS live fibroblasts. (**A**) Representative LSCM imaging of the TMRE-related fluorescence of euploid (N-HFF) and DS (NCDS-HFF and CDS-HFF) fibroblasts. The horizontal histograms on the right show the statistical analysis of the fluorescence intensity per cell as resulting from the averaged values ± SEM of about 100 randomly selected different cells for each sample from at least in-duplicate experiments. (**B**) Magnifications of intracellular selected details showing the mitochondrial functional network in representative samples of N-, NCDS- and CDS-HFF. A false-colours rendering of the TMRE-related fluorescence imaging is also shown.

that formed concentric layers instead of organizing into tubular cristae (28,29), leading to cristae patterns similar to those observed in DS samples. It is interesting to note that IMMT is significantly downregulated in DS fibroblasts.

Mitochondria have a key role in oxygen metabolism and subsequently they are the major source of ROS formation. Respirometry experiments conducted in this study demonstrated that in DS fibroblasts the OCR was significantly reduced in basal, uncoupled and ATP-synthase-dependent respiratory conditions, thus suggesting an impairment in oxidative phosphorylation competence, especially pronounced in DS fibroblasts from cardiopathic foeti. A correlation between the reduced respiratory activity and the morphological alterations in DS-HFF mitochondria indicates that the occurrence of de-structured cristae might partly account for the dysfunctioning oxidative phosphorylation in trisomic

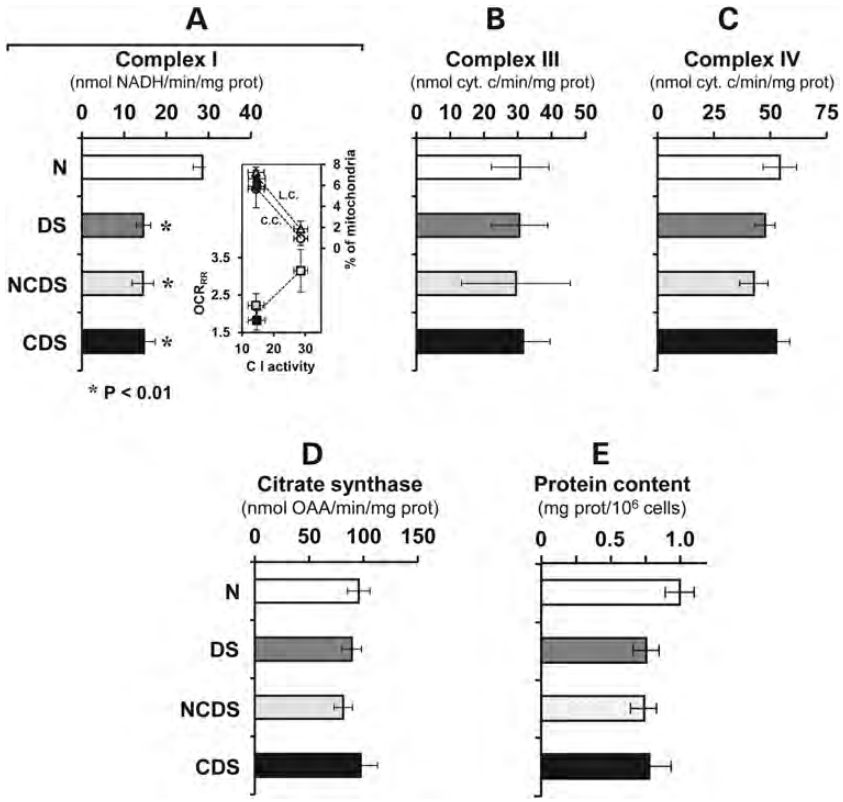

Figure 5. Enzymatic activities of the mitochondrial respiratory chain complexes of DS fibroblasts. The specific activities of (**A**) complex I (NADH-dehydrogenase), (**B**) complex III (cytochrome c reductase), (**C**) complex IV (cytochrome c reductase) were measured in cell lysates under conditions of saturating substrate as described in the Materials and Methods. The inset in (A) shows the correlation plot of the complex I activity versus either the OCR_{RR} (left Y axe) and the cristae morphological features (right Y axe; L.C., longitudinal cristae; C.C., concentric cristae); the values are means ± SEM of the clustered N-, NCDS- and CDS-HFF (same colour as the horizontal bars of the histogram). The citrate synthase activity, a marker of the mitochondrial content and the amount of protein per cell number are also shown in (**D**) and (**E**), respectively. N, DS, NCDS and CDS refer to the fibroblast sampling described in the legend of Figure 3; the bars are means ± SEM of the average determinations for each sample carried out in triplicate; when statistically significant, the difference when compared with the euploid samples is shown.

samples as also suggested by other authors (30,31). The analysis of individual complexes in the mitochondrial respiratory chain showed a strong reduction in the activity of complex I in DS fibroblasts irrespective of whether they were derived from cardiopathic trisomic foeti. Similar results have been recently reported (11). The authors attributed the reduced activity of complex I to defective cAMP/PKA-dependent phosphorylation. The impact of the OXPHOS decrease observed in DS fibroblasts did not result, however, in a severe bioenergetic failure compromising cell growth. This could be explained by an adaptive compensatory increase in the glycolytic flux, as shown in ref. (12), and by the gene-dosage effect of the Hsa21-harbored regulatory glycolytic enzyme phosphofructokinase PFKL (32).

In the present study, we observed a remarkable alteration in the redox homeostasis in DS-HFF highlighted by an increased production of ROS, which localized to an intracellular compartment resembling the mitochondrial network and was sensitive to the FCCP uncoupler and to the complex I inhibitor DPI. These two features would point to complex I as a major ROS generator in DS-HFF sustained by a 'forward electron transfer' mechanism (33,34). ROS production in DS-HFF was substantially suppressed by db-cAMP treatment, supporting the hypothesis that deregulation of post-translational modification of complex I is involved in the redox imbalance observed in DS-HFF.

A feature emerging from the present study is that the redox imbalance observed in DS-HFF was much larger in fibroblasts from cardiopathic foeti irrespective of the similar degree of inhibition of complex I in NCDS- and CDS-HFF. Release of ROS has been repetitively reported to be associated with an overload of Ca^{2+} into the mitochondria, although the mechanism remains to be satisfactorily explained (35,36). Consistent with this notion, we observed that DS-HFF displayed a higher steady level of intramitochondrial Ca^{2+} when compared with N-HFF, with the CDS-HFF exhibiting the highest $mtCa^{2+}$. A linear positive correlation was found between $mtCa^{2+}$ and ROS generation in the three cytotype samples. Most notably, blockage of the major mitochondrial Ca^{2+}-transporting system resulted in substantial depression of ROS overproduction in DS-HFF, whereas it was ineffective in N-HFF. Moreover, ruthenium red treatment resulted in full recovery of the respiratory activity in DS-HFF. All together, these observations would argue for a linkage between chronic intramitochondrial Ca^{2+} levels, inhibition of complex I and mitochondrial ROS production. Although

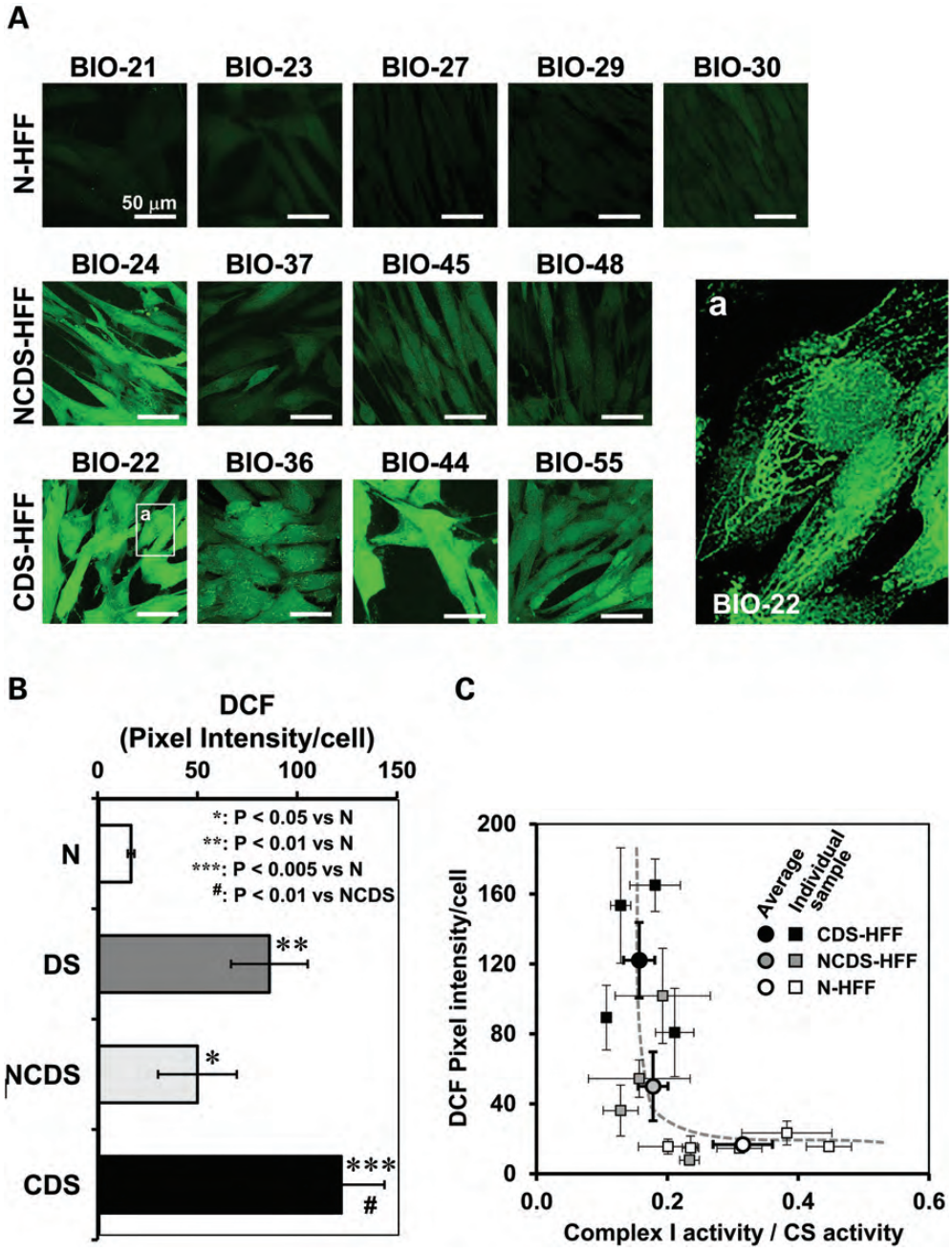

Figure 6. Confocal microscopy analysis of ROS production in DS live fibroblasts. (**A**) Representative LSCM imaging of the DCF-related fluorescence of euploid (N-HFF) and DS (NCDS-HFF and CDS-HFF) fibroblasts. A representative magnification of an intracellular selected detail (white rectangle) of the indicated CDS sample is shown displaying compartmentalization of the brighter DCF fluorescence signal. (**B**) Statistical analysis of the fluorescence intensity per cell as resulting from the averaged values ± SEM of about 100 randomly selected different cells for each sample from at least in-duplicate experiments; statistical analysis of the differences is also shown. (**C**) Correlation plot between the complex I activity normalized to the CS activity and the DCF-related fluorescence signal/cell for individual and averaged fibroblast samples (see symbol legend, means ± SEM).

we have not specifically addressed the cause of the Ca^{2+} homeostasis deregulation in trisomic cells, a survey of the literature suggests that cross-talk between PPARγ and Ca^{2+} mobilization/signalling (37) may be likely in this case. *PGC-1α* is an important coactivator of the *PPARs* transcription factor family, mainly *PPARγ* (38,39). Depression of *PGC-1α* activity, observed in DS-HFF samples, would consequently affect the transcriptional efficiency of *PPARs*-controlled genes.

PGC-1α function is both antagonized and regulated by a gene mapping to Hsa21, the nuclear receptor interacting protein *RIP140*. This highly conserved gene shows a 1.5- to 4-fold upregulation both in the heart and fibroblasts from DS subjects. The upregulation of *RIP140* protein was also demonstrated in the DS hippocampus (40). In the same experiment, the authors demonstrated that *SUMO3* (another gene mapping to Hsa21) is also upregulated in these cells. It was

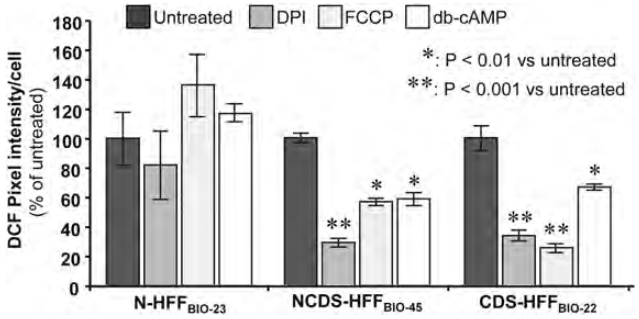

Figure 7. Effect of FCCP, DPI and db-cAMP on ROS production in DS fibroblasts. Cultured foetus-derived fibroblasts representative of euploid (BIO23) and DS non-cardiopathic (BIO45) or cardiopathic (BIO22) samples were treated for 2 h with either of 0.5 μM FCCP, 100 μM DPI or 100 μM db-cAMP and then assessed by LSCM for ROS production by DCF. The values shown are means ± SEM ($n = 3$ under each condition) of the DCF-related fluorescence intensity/cell normalized for each fibroblast sample to untreated cells. When statistically significant, the difference between untreated and compound-treated cells is reported.

demonstrated that the sumoylation of *RIP140* modulates its repressive activity (41). The simultaneous upregulation of both the Hsa21 genes, due to the primary dosage effect, might exert a synergistic effect. Silencing and re-expression experiments showed that *RIP140* expression significantly affects oxidative metabolism and mitochondrial biogenesis (42). Even mild *RIP140* overexpression repressed nuclear mitochondrial genes involved in all the respiratory chain complexes (43). We previously demonstrated that the same genes were repressed in DS foetal hearts (3).

Two other genes mapping to Hsa21, the kinase *DYRK1A* and the regulator of calcineurin 1 (*DSCR1/RCAN1*), were demonstrated to control *PGC-1α* via the *Calcineurin/NFAT* pathway, largely through the binding of *NFATc* to the *PGC-1α* promoter (44). The concurrent overexpression of the Hsa21 genes RIP140, SUMO3, *RCAN1* and *DYRK1A* and the downregulation of NFATc genes (45), observed in DS samples, is expected to result in the depression of *PGC-1α* expression.

In this study, we have demonstrated that some mitochondrial alterations are more pronounced in fibroblasts derived from DS foeti with heart defects. It must be pointed out that not all the subjects with trisomy 21 develop congenital cardiopathies, even though a heart developmental delay has been demonstrated in all DS human embryos at 8–10 gestational weeks (46). This suggests that a different inter-individual genetic background may affect the severity of the cardiopathic outcome in DS patients by impairing the oxidative metabolism. Assuming that altered cardiovascular development in DS likely originates from the trisomy of a critical Hsa21 region between *Tiam1* and *Kcnj6* (47), a more severe cardiac phenotype might be associated with different bioenergetic phenotypes characterized, at the cellular level, by a larger mitochondrial Ca^{2+} load and related ROS generation, as observed in CDS-HFF. Interesting is the evidence that the induction of oxidative stress in pregnant mice on day 7.5 disrupts cardiac neural crest migration and causes outflow tract defects like that observed in DS, and that antioxidant administration before the induction prevents the heart defects (48). Implications of our findings have a potential therapeutic value, as a number of drugs are becoming available to specifically inhibit the observed mitochondrial alterations. Some protocols are being developed to improve oxidative imbalance in DS using antioxidants such as the coenzyme Q10 (49,50). On the basis of our results, we also plan to investigate the effects of PPARγ agonists and/or of PGC-1α activators. The combination of these pharmacologically active compounds might correct mitochondria-related dysfunctions in trisomic foeti/patients.

MATERIALS AND METHODS

Ethics Statement

Human primary lines of HFF used in this study were obtained from the 'Telethon Bank of Fetal Biological Samples' at the University of Naples according to protocols approved by the local Institutional Ethics Committee.

Samples

Skin biopsies were explanted from 13 human foeti after therapeutic abortion at 18–22 gestational weeks and were classified as follows: five euploid human foeti (N-HFF) and eight foeti with trisomy of Hsa21 (DS-HFF) including four foeti with CHD, named CDS-HFF and four foeti without heart defects, named NCDS-HFF (Supplementary Material, Table S1). Fibroblasts from biopsies were cultured in T25 flasks (BD Falcon) with Chang medium B+C (Irvine Scientific) supplemented with 1% penicillin/streptomycin (Gibco) at 37°C in 5% CO_2 atmosphere; all the analyses described throughout this study were carried out at passages 4–5. Karyotype analysis was performed by standard G-banding technique.

The presence of CHD was established by colour Doppler foetal echocardiography followed by direct examination at the time of tissue explantation and dissection.

RNA extraction and quantitative real-time PCR

Total RNA from each sample was extracted using TRIzol reagent (Gibco/BRL Life Technologies, Inc., Gaithersburg, MD, USA) and was reverse-transcribed using the iScript cDNA Synthesis kit (Bio-Rad Laboratories Inc., Hercules, CA, USA). Real-time PCR was performed using iQ Supermix SYBR Green 2X on a Bio-Rad iCycler according to the manufacturer's protocols. PCR reactions were performed in triplicate. Primer pairs (MWG Biotech, Ebersberg, Germany) were designed using the Primer 3 software (http://frodo.wi.mit.edu/primer3) to obtain amplicons ranging from 100 to 150 bp (Supplementary Material, Table S2). *GAPDH* and *RPL13A* housekeeping genes were chosen as reference genes.

Morphological analysis

Fibroblasts from trisomic and euploid foeti were fixed and embedded for the electron microscope, using agarose as an intermediate embedding medium (51). Cells were fixed in petri dishes with 4% paraformaldehyde and 5% glutaraldehyde in PBS buffer (0.1 M, pH 7.3) for 30 min at room temperature,

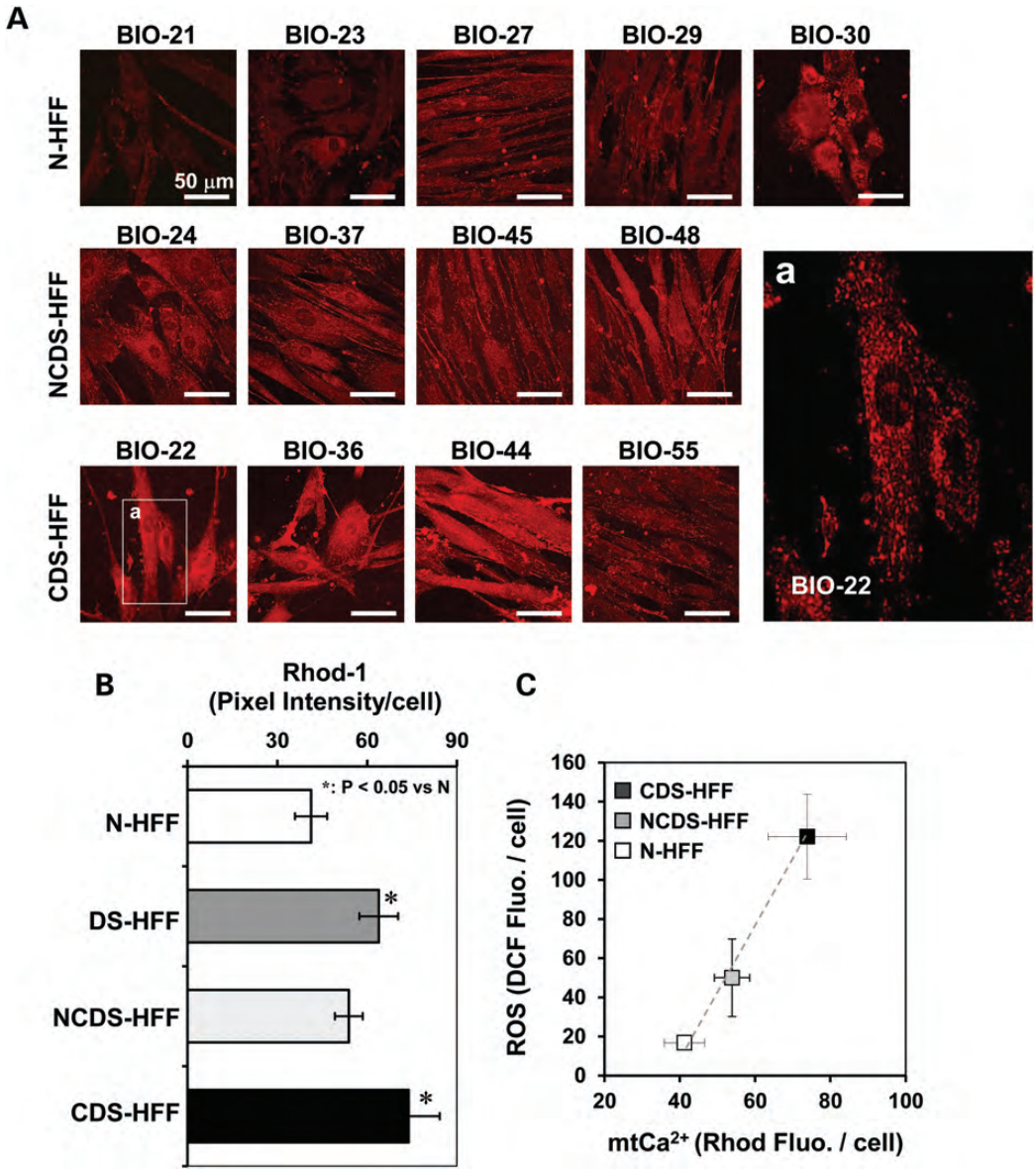

Figure 8. Confocal microscopy analysis of mitochondrial Ca^{2+} in DS live fibroblasts. (**A**) Representative LSCM imaging of the Rhod-1-related fluorescence of euploid (N-HFF) and DS (NCDS-HFF and CDS-HFF) fibroblasts. A representative magnification (white rectangle) of the indicated CDS sample is shown displaying the punctuate compartmentalization of the Rhod-1-fluorescence signal. (**B**) Statistical analysis of the fluorescence intensity per cell as resulting from the averaged values ± SEM of about 100 randomly selected different cells for each sample from at least in-duplicate experiments; when statistically significant, the difference when compared with the euploid samples is shown. (**C**) Correlation plot between the Rhod-1- and DCF-related fluorescence signal/cell for averaged fibroblast samples (see symbol legend, means ± SEM).

then washed in buffer, scraped from culture plates and pelleted by centrifugation for 10 min at 2000*g*; the supernatant was discarded and the cells were resuspended in 1 ml of 2% liquid agarose at 65°C. Again, the reaction tube was centrifuged for 5 min at 1000*g* to concentrate the cells in agarose. The agarose-cell pellet was solidified in ice for 30 min, and then the agarose cone was carefully taken out of the reaction tube and divided into small pieces (1 mm^3). The agarose-cell blocks were post-fixed in osmium tetroxide (1% in PBS buffer) for 1 h at 4°C, dehydrated and transferred first to propylene oxide, then to a mixture of propylene oxide-Epon (1:1) and finally embedded in Epon resin. The Epon blocks were polymerized for 2 days at 60°C and then sectioned with a diamond knife to give thin sections, 70–80 nm each; the sections were picked up on 200 mesh copper grids, stained with uranyl acetate (5% in 50% methanol) and Reynolds lead citrate (52) and observed on a Philips 208S transmission electron microscope. Micrographs were acquired with a Mega View II Soft Imaging System camera. Three N-HFF (BIO-21, BIO-23, BIO-27) and six DS-HFF samples (BIO24, BIO-36, BIO-37, BIO-44, BIO-48 and BIO55) were analysed using the 'fractionator' method to obtain a systematic and uniformly random sampling, which ensures that even for relatively small samples, the error is so small that it may safely be ignored (53). Fifty cells per sample were analysed and for each cell the percentages of inner and outer membrane

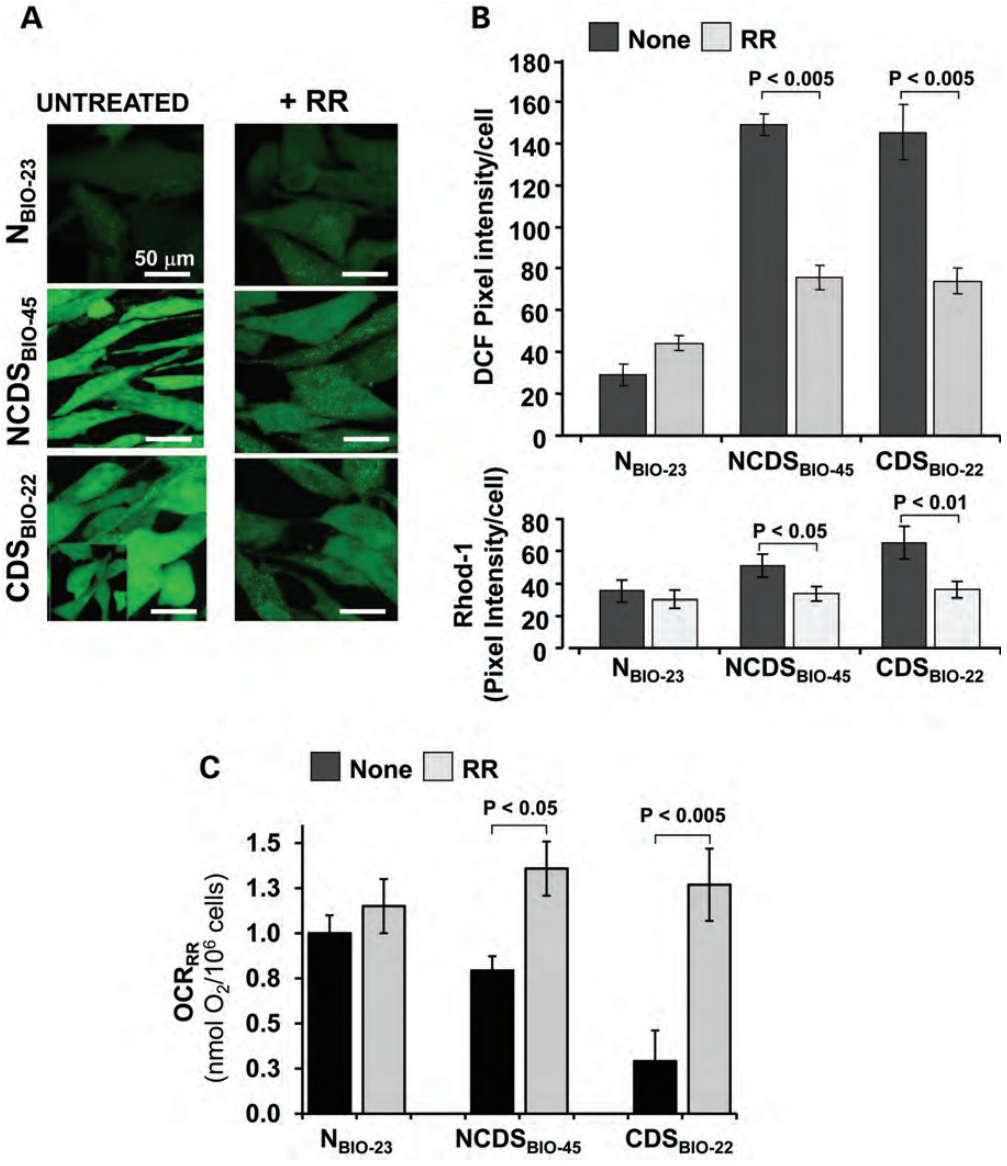

Figure 9. Effect of ruthenium red on ROS production and respiratory activity in DS live fibroblasts. Cultured foetus-derived fibroblasts representative of euploid (BIO23) and DS non-cardiopathic (BIO45) or cardiopathic (BIO22) samples were treated with 10 μM ruthenium red (RR) for 4 h and then assessed by LSCM for ROS production and $mtCa^{2+}$ by DCF and Rhod-1, respectively. (**A**) DCF-related fluorescence imaging of untreated and RR-treated fibroblasts (representative of three different experiments). (**B**) Statistical analysis of the DCF-related (upper histogram) and Rhod-1-related (lower histogram) fluorescence intensity per cell. The average values ± SEM of about 100 randomly selected different cells for each sample from three different experiments are shown. (**C**) Effect of RR on the respiratory activity of the same representative samples of N-, NCDS- and CDS-HFF as in (A). The OCR_{RR} was measured as described in the legend of Figure 3 and treatment with RR as in (A); the bars are means ± SEM of the average determinations for each sample (untreated and RR-treated) carried out in triplicate. When statistically significant, the difference between untreated and RR-treated cells is reported in (B) and (C).

breakages, branched mitochondria and mitochondria with concentric or longitudinal cristae were determined. Furthermore, for each sample, 25 micrographs were collected to evaluate the mitochondrial volume density (Vmt, relative volume of mitochondria on cell volume) and mitochondrial cristae volume density (Vmc, relative volume of mitochondrial cristae on mitochondria volume) (54). The volume density (also named relative volume or volume fraction) is a ratio between volumes. This is an intuitive parameter, unbiasedly estimated by overlaying a test system of points on images and then counting those falling over the objects of interest and those over the reference space. The ratio of points gives the estimation of volume. According to Delesse's principle, the volume fraction of an object varies proportionally to their area fraction as measured in random 2D sections; this means that each point controls an area in a 2D section and is related to a defined volume in the 3D organ (55).

Western blot analysis

Cells were washed twice with ice-cold PBS and lysed in RIPA buffer (NaCl 154 mM; Deoxicolic Acid 12 mM; NaF 0.95 mM;

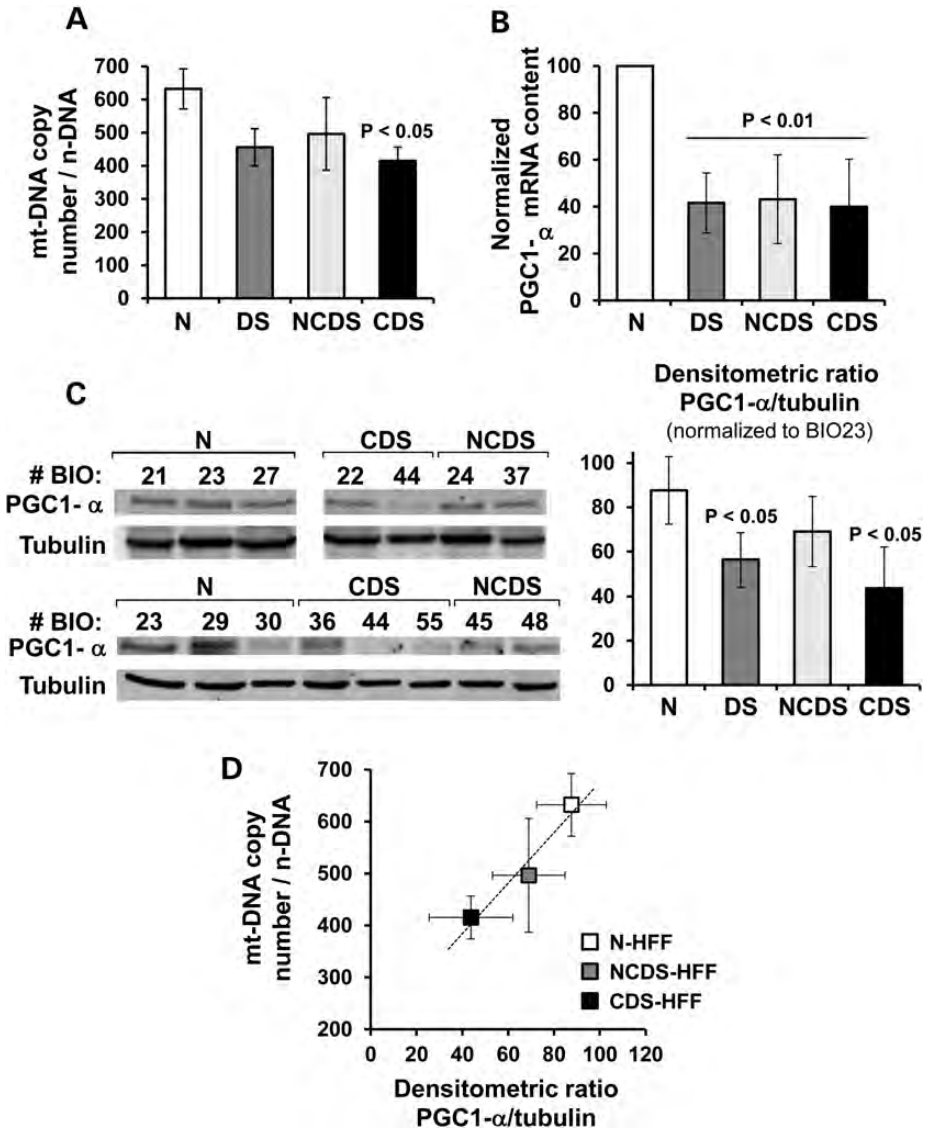

Figure 10. Analysis of the mitochondrial DNA content and expression of PGC-1α in DS fibroblasts. (**A**) Absolute qRT-PCR analysis of mtDNA (see Materials and Methods for details). The bars are means ± SEM from five euploid and eight DS fibroblast samples; a distinction between non-cardiopathic (NCDS, $n = 4$) and cardiopathic (CDS, $n = 4$) foetus-derived fibroblasts is also reported. (**B**) Expression analysis of the PGC-1α by qRT-PCR. The values, means ± SEM, of the DS samples are normalized to that of the euploid fibroblasts. (**C**) Analysis of the PGC-1α protein. (Panel on the left) Western blotting of PGC-1α on total cellular protein extracts from euploid and DS samples (representative of two to three different analyses carried out for each sample). (Panel on the right) Densitometric analysis of the PGC-1α-related immunodetected bands (means ± SEM of two to three assays). To compare different electrophoretic runs, the densitometric value (normalized to tubulin) of the euploid sample BIO-23 was taken as an internal reference. When statistically significant, the *P*-value, when compared with the euploid samples, is shown in (A and B) and (C and **D**) Correlation plot between the normalized PGC-1α protein expression and the mt-DNA copy number for averaged fibroblast samples (see symbol legend, means ± SEM).

Triton X-100 1%; SDS 2%; PMSF 2 mM) in phosphate buffer in the presence of protease inhibitors. The protein concentration was determined using the Bio-Rad protein assay (Bio-Rad Laboratories Inc.). For western blot analysis, total lysates were boiled for 5 min in Laemmli sample buffer and analysed on 7.5% SDS–PAGE. Gels were then blotted onto nitrocellulose transfer membranes (Schleicher and Shuell GmbH, Dassel, Germany) using a Bio-Rad apparatus. After transfer, the filters were blocked at room temperature for 1 h with 5% BSA in TTBS (150 mM NaCl, 20 mM Tris-HCl pH 7.5). After washing twice with TTBS (150 mM NaCl, 20 mM Tris-HCl pH 7.5, 0.1% Tween 20), filters were incubated overnight at 4°C with rabbit polyclonal primary antibody to *PGC-1α* (1:1000, Abcam, Cambridge Science Park, Cambridge, UK). The filters were washed extensively with TTBS and incubated for 1 h at room temperature with anti-rabbit peroxidase-conjugated secondary antibody (Amersham, Little Chalfont, Buckinghamshire, UK) diluted 1:1000 in TTBS. The filters were then washed six times with TTBS and once with TBS and developed using an ECL western blotting substrate detection method (Pierce, Rockford, IL, USA). For reprobing, the nitrocellulose filters were re-hydrated and

stripped for 30 min at 37°C in restore western blotting stripping buffer (Pierce) and washed extensively with TTBS. Results were standardized to alpha tubulin and analysed using NIH Image J (Rasband, W.S., ImageJ, U. S. National Institutes of Health, Bethesda, Maryland, USA, http://imagej.nih.gov/ij/, 1997–2012).

Measurement of the respiratory activity in intact cells

Cultured cells were gently detached from the dish by tripsinization, washed in PBS, harvested by centrifugation at 500*g* for 5 min and immediately assessed for O_2 consumption with a high-resolution oxymeter (Oxygraph-2k, Oroboros Instruments). About 1×10^6 viable cells per ml were assayed in 50 mM KPi, 10 mM Hepes, 1 mM EDTA, pH 7.4 at 37°C; after attainment of a stationary endogenous substrate-sustained resting oxygen consumption rate (OCR_{RR}), 2 μg/ml of the ATP-synthase inhibitor oligomycin was added (OCR_{OL}) followed by addition of 0.5 mM of the uncoupler carbonilcyanide p-triflouromethoxyphenylhydrazone (FCCP) (OCR_{UNC}). The rates of oxygen consumption were corrected for 2 mM KCN-insensitive respiration. The RCR was obtained by the ratio OCR_{UNC}/OCR_{OL}, the leak by the ratio OCR_{OL}/OCR_{UNC} and the ATP-synthesis-linked respiration (OXPHOS) by the ratio $(OCR_{RR}\text{-}OCR_{OL})/OCR_{UNC}$ (56).

Measurement of the activity of mitochondrial respiratory chain complexes

The specific activities of NADH:ubiquinone oxidoreductase (complex I), ubiquinone:cytochrome c oxidoreductase (complex III) and cytochrome c oxidase (complex IV) were assayed spectrophotometrically on frozen-thawn and ultrasound-treated cells in 10 mM Tris, 1 mg/ml serum albumin, pH 8.0. Complex I was assayed (in the presence of 1 μg/ml of antymicin A *plus* 2 mM KCN) by following the initial 2 μg/ml rotenone-sensitive rate of 50 μM NADH oxidation ($\varepsilon_{340nm} = 6.22\ mM^{-1}\ cm^{-1}$) in the presence of 200 μM decylubiquinone (dUQ) as electron acceptor; complex III was assayed (in the presence of rotenone *plus* KCN) by following the initial 1 μg/ml antymicin A-sensitive rate of 50 μM ferri-cytochrome *c* reduction ($\varepsilon_{550nm} = 21.1\ mM^{-1}\ cm^{-1}$) in the presence of 200 μM $dUQH_2$ as electron donor. Complex IV was assayed by following (in the presence of antymicin A) the initial 2 mM KCN-sensitive rate of 20 μM ferro-cytochrome *c* oxidation under aerobic conditions. The activities were normalized to the initial cell number and to cellular protein content (57). Citrate synthase catalyses the reaction between acetyl coenzyme A and oxaloacetic acid to form citric acid. Citrate synthase activity was assayed spectrophotometrically ($\varepsilon_{412nm} = 13.6\ mM^{-1}\ cm^{-1}$) measuring the reaction between CoA-SH and DTNB (5,5′-dithiobis (2-nitrobenzoic acid)) to form 5-thio-2-nitrobenzoic acid (TNB) (58).

Laser scanning confocal microscopy (LSCM) live cell imaging of mitochondrial membrane potential, ROS and $mtCa^{2+}$

Cells cultured at low density on fibronectin-coated 35-mm glass-bottom dishes were incubated for 20 min at 37°C with the either of the following probes: 2 μM tetramethylrhodamine ethyl ester (TMRE) to monitor mitochondrial membrane potential ($\Delta\Psi_m$); 10 μM 2,7-dichlorofluorescin diacetate, which is converted to dichlorofluorescein by intracellular esterases, for detection of H_2O_2; 5 μM X-Rhod-1 AM for mitochondrial Ca^{2+}. All probes were from Molecular Probes (Eugene, OR). Stained cells were washed with PBS and examined with a Nikon TE 2000 microscope [images collected using a ×60 objective (1.4 NA)] coupled to a Radiance 2100 dual-laser LSCM system (Bio-Rad). TMRE and Rhod-1 red fluorescence were elicited by exciting with the He–Ne laser beam (λex 543 nm), whereas dichlorofluorescein green fluorescence was elicited with the Ar–Kr laser beam (λex 488 nm). Acquisition, storage and analysis of data were performed with LaserSharp and LaserPix software from Bio-Rad or ImageJ version 1.37. Superimposed confocal planes were analysed by means of the 'stack' function of the LCS-Analysis Tools, which produced an *xz* intensity profile of the average value of the pixels within marked edges, including a single cell, as a function of each focal plane. The integrated value of the *xz* profile was taken as a measure of the fluorescence intensity of that individual cell relative to the selected emission channel. Correction was made for the minimal background by repeating the procedure in a cell-free field. About 100 single cells were analysed for each imaging analysis (57).

Statistics

The ANOVA test with Bonferroni *post hoc* correction was applied to evaluate the statistical significance of differences measured throughout the data sets presented. Concerning stereological investigations, the data obtained from each sample were averaged per group (N-HFF, DS-HFF, NCDS-HFF and CDS-HFF) and statistical evaluations were performed by using two nonparametric statistical tests, the Kolmogorov–Smirnov and the Kruskal–Wallis tests. The threshold for statistical significance (*P*-value) was set to 0.05.

SUPPLEMENTARY MATERIAL

Supplementary Material is available at *HMG* online.

Conflict of Interest statement. None declared.

FUNDING

This work was supported by grants from Campania Region (POR CREME to L.N.) and from the Italian Ministry of University and Research (PRIN-2008FJJHKM_001 to N.C.).

REFERENCES

1. Epstein, C.J., Korenberg, J.R., Anneren, G., Antonarakis, S.E., Ayme, S., Courchesne, E., Epstein, L.B., Fowler, A., Groner, Y., Huret, J.L *et al.* (1991) Protocols to establish genotype-phenotype correlations in Down syndrome. *Am. J. Hum. Genet.*, **49**, 207–235.
2. Park, S.C., Mathews, R.A., Zuberbuhler, J.R., Rowe, R.D., Neches, W.H. and Lenox, C.C. (1977) Down syndrome with congenital heart malformation. *Am. J. Dis. Child*, **131**, 29–33.

3. Conti, A., Fabbrini, F., D'Agostino, P., Negri, R., Greco, D., Genesio, R., D'Armiento, M., Olla, C., Paladini, D., Zannini, M *et al.* (2007) Altered expression of mitochondrial and extracellular matrix genes in the heart of human fetuses with chromosome 21 trisomy. *BMC Genomics*, **8**, 268.
4. Busciglio, J. and Yankner, B.A. (1995) Apoptosis and increased generation of reactive oxygen species in Down's syndrome neurons in vitro. *Nature*, **378**, 776–779.
5. Busciglio, J., Pelsman, A., Wong, C., Pigino, G., Yuan, M., Mori, H. and Yankner, B.A. (2002) Altered metabolism of the amyloid beta precursor protein is associated with mitochondrial dysfunction in Down's syndrome. *Neuron*, **33**, 677–688.
6. Roat, E., Prada, N., Ferraresi, R., Giovenzana, C., Nasi, M., Troiano, L., Pinti, M., Nemes, E., Lugli, E., Biagioni, O *et al.* (2007) Mitochondrial alterations and tendency to apoptosis in peripheral blood cells from children with Down syndrome. *FEBS Lett.*, **581**, 521–525.
7. Schuchmann, S. and Heinemann, U. (2000) Increased mitochondrial superoxide generation in neurons from trisomy 16 mice: a model of Down's syndrome. *Free Radic. Biol. Med.*, **28**, 235–250.
8. Shukkur, E.A., Shimohata, A., Akagi, T., Yu, W., Yamaguchi, M., Murayama, M., Chui, D., Takeuchi, T., Amano, K., Subramhanya, K.H *et al.* (2006) Mitochondrial dysfunction and tau hyperphosphorylation in Ts1Cje, a mouse model for Down syndrome. *Hum. Mol. Genet.*, **15**, 2752–2762.
9. Kim, S.H., Vlkolinsky, R., Cairns, N., Fountoulakis, M. and Lubec, G. (2001) The reduction of NADH ubiquinone oxidoreductase 24- and 75-kDa subunits in brains of patients with Down syndrome and Alzheimer's disease. *Life Sci.*, **68**, 2741–2750.
10. Bambrick, L.L. and Fiskum, G. (2008) Mitochondrial dysfunction in mouse trisomy 16 brain. *Brain Res.*, **1188**, 9–16.
11. Valenti, D., Manente, G.A., Moro, L., Marra, E. and Vacca, R.A. (2011) Deficit of complex I activity in human skin fibroblasts with chromosome 21 trisomy and overproduction of reactive oxygen species by mitochondria: involvement of the cAMP/PKA signalling pathway. *Biochem. J.*, **435**, 679–688.
12. Valenti, D., Tullo, A., Caratozzolo, M.F., Merafina, R.S., Scartezzini, P., Marra, E. and Vacca, R.A. (2010) Impairment of F1F0-ATPase, adenine nucleotide translocator and adenylate kinase causes mitochondrial energy deficit in human skin fibroblasts with chromosome 21 trisomy. *Biochem. J.*, **431**, 299–310.
13. Scarpulla, R.C. (2011) Metabolic control of mitochondrial biogenesis through the PGC-1 family regulatory network. *Biochim. Biophys. Acta*, **1813**, 1269–1278.
14. Mao, R., Wang, X., Spitznagel, E.L. Jr, Frelin, L.P., Ting, J.C., Ding, H., Kim, J.W., Ruczinski, I., Downey, T.J. and Pevsner, J. (2005) Primary and secondary transcriptional effects in the developing human Down syndrome brain and heart. *Genome Biol.*, **6**, R107.
15. Sharma, L.K., Lu, J. and Bai, Y. (2009) Mitochondrial respiratory complex I: structure, function and implication in human diseases. *Curr. Med. Chem.*, **16**, 1266–1277.
16. Bellomo, F., Piccoli, C., Cocco, T., Scacco, S., Papa, F., Gaballo, A., Boffoli, D., Signorile, A., D'Aprile, A., Scrima, R *et al.* (2006) Regulation by the cAMP cascade of oxygen free radical balance in mammalian cells. *Antioxid. Redox Signal*, **8**, 495–502.
17. Papa, S., Rasmo, D.D., Technikova-Dobrova, Z., Panelli, D., Signorile, A., Scacco, S., Petruzzella, V., Papa, F., Palmisano, G., Gnoni, A *et al.* (2012) Respiratory chain complex I, a main regulatory target of the cAMP/PKA pathway is defective in different human diseases. *FEBS Lett.*, **586**, 568–577.
18. Caviedes, P., Caviedes, R. and Rapoport, S.I. (2006) Altered calcium currents in cultured sensory neurons of normal and trisomy 16 mouse fetuses, an animal model for human trisomy 21 (Down syndrome). *Biol. Res.*, **39**, 471–481.
19. Li, H., Rao, A. and Hogan, P.G. (2011) Interaction of calcineurin with substrates and targeting proteins. *Trends Cell Biol.*, **21**, 91–103.
20. Yamato, F., Takaya, J., Yasuhara, A., Teraguchi, M., Ikemoto, Y. and Kaneko, K. (2009) Elevated intracellular calcium in neutrophils in patients with Down syndrome. *Pediatr. Int.*, **51**, 474–477.
21. De Stefani, D., Raffaello, A., Teardo, E., Szabo, I. and Rizzuto, R. (2011) A forty-kilodalton protein of the inner membrane is the mitochondrial calcium uniporter. *Nature*, **476**, 336–340.
22. Drago, I., Pizzo, P. and Pozzan, T. (2011) After half a century mitochondrial calcium in- and efflux machineries reveal themselves. *EMBO J.*, **30**, 4119–4125.
23. Peng, T.I. and Jou, M.J. (2010) Oxidative stress caused by mitochondrial calcium overload. *Ann. N. Y. Acad. Sci.*, **1201**, 183–188.
24. Chen, Y., Wang, Y., Chen, J., Chen, X., Cao, W., Chen, S., Xu, S., Huang, H. and Liu, P. (2012) Roles of transcriptional corepressor RIP140 and coactivator PGC-1alpha in energy state of chronically infarcted rat hearts and mitochondrial function of cardiomyocytes. *Mol. Cell. Endocrinol.*, **362**, 11–18.
25. Leone, T.C., Lehman, J.J., Finck, B.N., Schaeffer, P.J., Wende, A.R., Boudina, S., Courtois, M., Wozniak, D.F., Sambandam, N., Bernal-Mizrachi, C *et al.*. (2005) PGC-1alpha deficiency causes multi-system energy metabolic derangements: muscle dysfunction, abnormal weight control and hepatic steatosis. *PLoS Biol.*, **3**, e101.
26. Mitra, R., Nogee, D.P., Zechner, J.F., Yea, K., Gierasch, C.M., Kovacs, A., Medeiros, D.M., Kelly, D.P. and Duncan, J.G. (2012) The transcriptional coactivators, PGC-1alpha and beta, cooperate to maintain cardiac mitochondrial function during the early stages of insulin resistance. *J. Mol. Cell. Cardiol.*, **52**, 701–710.
27. Bersu, E.T., Ahmad, F.J., Schwei, M.J. and Baas, P.W. (1998) Cytoplasmic abnormalities in cultured cerebellar neurons from the trisomy 16 mouse. *Brain Res. Dev. Brain Res.*, **109**, 115–120.
28. John, G.B., Shang, Y., Li, L., Renken, C., Mannella, C.A., Selker, J.M., Rangell, L., Bennett, M.J. and Zha, J. (2005) The mitochondrial inner membrane protein mitofilin controls cristae morphology. *Mol. Biol. Cell*, **16**, 1543–1554.
29. Zerbes, R.M., Bohnert, M., Stroud, D.A., von der Malsburg, K., Kram, A., Oeljeklaus, S., Warscheid, B., Becker, T., Wiedemann, N., Veenhuis, M *et al.* (2012) Role of MINOS in mitochondrial membrane architecture: cristae morphology and outer membrane interactions differentially depend on mitofilin domains. *J. Mol. Biol.*, **422**, 183–191.
30. Darshi, M., Mendiola, V.L., Mackey, M.R., Murphy, A.N., Koller, A., Perkins, G.A., Ellisman, M.H. and Taylor, S.S. (2011) ChChd3, an inner mitochondrial membrane protein, is essential for maintaining crista integrity and mitochondrial function. *J. Biol. Chem.*, **286**, 2918–2932.
31. Zick, M., Rabl, R. and Reichert, A.S. (2009) Cristae formation-linking ultrastructure and function of mitochondria. *Biochim. Biophys. Acta*, **1793**, 5–19.
32. Lambert, A.J., Buckingham, J.A., Boysen, H.M. and Brand, M.D. (2008) Diphenyleneiodonium acutely inhibits reactive oxygen species production by mitochondrial complex I during reverse, but not forward electron transport. *Biochim. Biophys. Acta*, **1777**, 397–403.
33. Annerén, K.G., Korenberg, J.R. and Epstein, C.J. (1987) Phosphofructokinase activity in fibroblasts aneuploid for chromosome 21. *Hum. Genet.*, **76**, 63–65.
34. Selivanov, V.A., Votyakova, T.V., Pivtoraiko, V.N., Zeak, J., Sukhomlin, T., Trucco, M., Roca, J. and Cascante, M. (2011) Reactive oxygen species production by forward and reverse electron fluxes in the mitochondrial respiratory chain. *PLoS Comput. Biol.*, **7**, e1001115.
35. Adam-Vizi, V. and Starkov, A.A. (2010) Calcium and mitochondrial reactive oxygen species generation: how to read the facts. *J. Alzheimer Dis.*, **20**(Suppl. 2), S413–S426.
36. Feissner, R.F., Skalska, J., Gaum, W.E. and Sheu, S.S. (2009) Crosstalk signaling between mitochondrial Ca2+ and ROS. *Front. Biosci.*, **14**, 1197–1218.
37. Bush, C.R., Havens, J.M., Necela, B.M., Su, W., Chen, L., Yanagisawa, M., Anastasiadis, P.Z., Guerra, R., Luxon, B.A. and Thompson, E.A. (2007) Functional genomic analysis reveals cross-talk between peroxisome proliferator-activated receptor gamma and calcium signaling in human colorectal cancer cells. *J. Biol. Chem.*, **282**, 23387–23401.
38. Oyekan, A. (2011) PPARs and their effects on the cardiovascular system. *Clin. Exp. Hypertens*, **33**, 287–293.
39. Puigserver, P., Wu, Z., Park, C.W., Graves, R., Wright, M. and Spiegelman, B.M. (1998) A cold-inducible coactivator of nuclear receptors linked to adaptive thermogenesis. *Cell*, **92**, 829–839.
40. Gardiner, K. (2006) Transcriptional dysregulation in Down syndrome: predictions for altered protein complex stoichiometries and post-translational modifications, and consequences for learning/behavior genes ELK, CREB, and the estrogen and glucocorticoid receptors. *Behav. Genet.*, **36**, 439–453.
41. Rytinki, M.M. and Palvimo, J.J. (2009) SUMOylation attenuates the function of PGC-1alpha. *J. Biol. Chem.*, **284**, 26184–26193.
42. Powelka, A.M., Seth, A., Virbasius, J.V., Kiskinis, E., Nicoloro, S.M., Guilherme, A., Tang, X., Straubhaar, J., Cherniack, A.D., Parker, M.G *et al.* (2006) Suppression of oxidative metabolism and mitochondrial

biogenesis by the transcriptional corepressor RIP140 in mouse adipocytes. *J. Clin. Invest.*, **116**, 125–136.
43. Seth, A., Steel, J.H., Nichol, D., Pocock, V., Kumaran, M.K., Fritah, A., Mobberley, M., Ryder, T.A., Rowlerson, A., Scott, J *et al.* (2007) The transcriptional corepressor RIP140 regulates oxidative metabolism in skeletal muscle. *Cell Metab.*, **6**, 236–245.
44. Handschin, C., Rhee, J., Lin, J., Tarr, P.T. and Spiegelman, B.M. (2003) An autoregulatory loop controls peroxisome proliferator-activated receptor gamma coactivator 1alpha expression in muscle. *Proc. Natl Acad. Sci. USA*, **100**, 7111–7116.
45. Arron, J.R., Winslow, M.M., Polleri, A., Chang, C.P., Wu, H., Gao, X., Neilson, J.R., Chen, L., Heit, J.J., Kim, S.K *et al.* (2006) NFAT dysregulation by increased dosage of DSCR1 and DYRK1A on chromosome 21. *Nature*, **441**, 595–600.
46. Gittenberger-de Groot, A.C., Bartram, U., Oosthoek, P.W., Bartelings, M.M., Hogers, B., Poelmann, R.E., Jongewaard, I.N. and Klewer, S.E. (2003) Collagen type VI expression during cardiac development and in human fetuses with trisomy 21. *Anat. Rec. A Discov. Mol. Cell. Evol. Biol.*, **275**, 1109–1116.
47. Liu, C., Morishima, M., Yu, T., Matsui, S., Zhang, L., Fu, D., Pao, A., Costa, A.C., Gardiner, K.J., Cowell, J.K *et al.* (2011) Genetic analysis of Down syndrome-associated heart defects in mice. *Hum. Genet.*, **130**, 623–632.
48. Morgan, S.C., Relaix, F., Sandell, L.L. and Loeken, M.R. (2008) Oxidative stress during diabetic pregnancy disrupts cardiac neural crest migration and causes outflow tract defects. *Birth Defects Res. A Clin. Mol. Teratol.*, **82**, 453–463.
49. Miles, M.V., Patterson, B.J., Chalfonte-Evans, M.L., Horn, P.S., Hickey, F.J., Schapiro, M.B., Steele, P.E., Tang, P.H. and Hotze, S.L. (2007) Coenzyme Q10 (ubiquinol-10) supplementation improves oxidative imbalance in children with trisomy 21. *Pediatr. Neurol.*, **37**, 398–403.
50. Tiano, L., Carnevali, P., Padella, L., Santoro, L., Principi, F., Bruge, F., Carle, F., Gesuita, R., Gabrielli, O. and Littarru, G.P. (2011) Effect of Coenzyme Q10 in mitigating oxidative DNA damage in Down syndrome patients, a double blind randomized controlled trial. *Neurobiol. Aging*, **32**, 2103–2105.
51. Kerstens, H.M., Robben, J.C., Poddighe, P.J., Melchers, W.J., Boonstra, H., de Wilde, P.C., Macville, M.V. and Hanselaar, A.G. (2000) AgarCyto: a novel cell-processing method for multiple molecular diagnostic analyses of the uterine cervix. *J. Histochem. Cytochem.*, **48**, 709–718.
52. Reynolds, E.S. (1963) The use of lead citrate at high pH as an electron-opaque stain in electron microscopy. *J. Cell Biol.*, **17**, 208–212.
53. Gundersen, H.J. (2002) The smooth fractionator. *J. Microsc.*, **207**, 191–210.
54. Weibel, E.R., Kistler, G.S. and Scherle, W.F. (1966) Practical stereological methods for morphometric cytology. *J. Cell Biol.*, **30**, 23–38.
55. Marcos, R., Monteiro, R.A. and Rocha, E. (2012) The use of design-based stereology to evaluate volumes and numbers in the liver: a review with practical guidelines. *J. Anat.*, **220**, 303–317.
56. Piccoli, C., Scrima, R., Quarato, G., D'Aprile, A., Ripoli, M., Lecce, L., Boffoli, D., Moradpour, D. and Capitanio, N. (2007) Hepatitis C virus protein expression causes calcium-mediated mitochondrial bioenergetic dysfunction and nitro-oxidative stress. *Hepatology*, **46**, 58–65.
57. Cela, O., Piccoli, C., Scrima, R., Quarato, G., Marolla, A., Cinnella, G., Dambrosio, M. and Capitanio, N. (2010) Bupivacaine uncouples the mitochondrial oxidative phosphorylation, inhibits respiratory chain complexes I and III and enhances ROS production: results of a study on cell cultures. *Mitochondrion*, **10**, 487–496.
58. Barrientos, A., Fontanesi, F. and Diaz, F. (2009) Evaluation of the mitochondrial respiratory chain and oxidative phosphorylation system using polarography and spectrophotometric enzyme assays. *Curr. Protoc. Hum. Genet.*, **Chapter 19**, Unit19.13.